crystals

MDPI

Article

(Ba,K)(Zn,Mn)$_2$Sb$_2$: A New Type of Diluted Magnetic Semiconductor

Shuang Yu [1,2], Guoqiang Zhao [1,2], Yi Peng [1,2], Xiancheng Wang [1,2], Qingqing Liu [1,2], Runze Yu [1,2], Sijia Zhang [1,2], Jianfa Zhao [1,2,3], Wenmin Li [1,2], Zheng Deng [1,2,*], Yasutomo J. Uemura [4] and Changqing Jin [1,2,3,*]

1 Beijing National Laboratory for Condensed Matter Physics, and Institute of Physics, Chinese Academy of Sciences, Beijing 100190, China; yushuang@iphy.ac.cn (S.Y.); g.q.zhao@iphy.ac.cn (G.Z.); ypeng@iphy.ac.cn (Y.P.); wangxiancheng@aphy.iphy.ac.cn (X.W.); qqliu@aphy.iphy.ac.cn (Q.L.); yurz@iphy.ac.cn (R.Y.); sjzhang@iphy.ac.cn (S.Z.); zhaojf@iphy.ac.cn (J.Z.); liwenmin12@mails.ucas.ac.cn (W.L.)
2 School of Physics, University of Chinese Academy of Sciences, Beijing 100190, China
3 Materials Research Lab at Songshan Lake, Dongguan 523808, China
4 Department of Physics, Columbia University, New York, NY 10027, USA; tomo@lorentz.phys.columbia.edu
* Correspondence: dengzheng@iphy.ac.cn (Z.D.); Jin@iphy.ac.cn (C.J.); Tel.: +86-10-82648041 (Z.D.); +86-10-82649163 (C.J.)

Received: 28 June 2020; Accepted: 6 August 2020; Published: 10 August 2020

Abstract: A series of polycrystalline samples of a new diluted magnetic semiconductor (DMS) (Ba,K)(Zn,Mn)$_2$Sb$_2$ has been synthesized and systematically studied. The parent phase is the so-called "Zintl compound" BaZn$_2$Sb$_2$, a week-degenerate semiconductor with a narrow band gap of 0.2 eV. In (Ba,K)(Zn,Mn)$_2$Sb$_2$, the charge is doped by (Ba,K) substitution while the spin is independently doped by (Zn,Mn) substitution. (Ba,K)(Zn,Mn)$_2$Sb$_2$ and analogue (Ba,K)(Zn,Mn)$_2$As$_2$ have comparable narrow band gaps, carrier and spin concentrations. However, the former establishes a short-range spin-glass order at a very low temperature (<10 K), while the latter forms a long-range ferromagnetic ordering with a Curie temperature up to 230 K. The sharp contrast makes (Ba,K)(Zn,Mn)$_2$Sb$_2$ to be a touchstone for DMS theoretical models.

Keywords: diluted magnetic semiconductor; independent charge and spin doping; spin-glass behaviors; large magnetoresistance

1. Introduction

Dilute magnetic semiconductors (DMS) which have potential to control charge and spin in a single material are very applicable to spintronic devices [1–3]. Since the discovery of (Ga,Mn)As and (In,Mn)As, the III–V-based DMS have receive much attention as prototypical DMS materials [4]. However, in either (Ga,Mn)As or (In,Mn)As, heterovalent (Ga^{3+},Mn^{2+}) or (In^{3+},Mn^{2+}) substitution leads to difficulties in the individual control of carrier and spin doping and seriously limited chemical solubility. These two obstacles prevent further improving Curie temperature (T_C) in the III–V based DMS.

Recently, a series of new DMS materials with the independent doping of carrier and spin have been discovered, e.g., "111" type Li(Zn,Mn)As and "122" type (Ba,K)(Zn,Mn)$_2$As$_2$ [5–13]. A large number of progresses have been made in these new DMS, in both fundamental studies and potential applications [14–28]. Among the new DMS, (Ba,K)(Zn,Mn)$_2$As$_2$ has a maximum Curie temperature (T_C) of 230 K, which is a reliable record of carrier-mediated ferromagnetic DMS [29,30]. Besides, the physical picture of (Ba,K)(Zn,Mn)$_2$As$_2$ is believed to be general and thus applicable to other DMS [31–33].

(Ba,K)(Zn,Mn)$_2$As$_2$ stimulates further searching for DMS with a T_C over room temperature. Recent theoretical calculations predicted that the Curie temperature of (Ba,K)(Zn,Mn)$_2$Sb$_2$ is even

higher than 230 K [34]. (Ba,K)(Zn,Mn)$_2$Sb$_2$ does not contain a toxic element, another advantage over (Ba,K)(Zn,Mn)$_2$As$_2$. As reported, it has a band gap of 0.2 eV, similar to that of (Ba,K)(Zn,Mn)$_2$As$_2$. In this paper, we report the synthesis and physical properties of K- and Mn-co-doped (Ba,K)(Zn,Mn)$_2$Sb$_2$.

2. Experimental

Polycrystalline specimens of $(Ba_{1-x}K_x)(Zn_{1-y}Mn_y)_2Sb_2$ were synthesized with a solid state reaction method. The high purity of raw materials, Ba, K, Zn, Mn and Sb, were well ground according to the stoichiometric ratio, and then pressed into pellets. The pellets were sealed into Ta tube and heated to 750 K for 10 h before cooling down to room temperature. All the procedures are protected under high purity argon. Powder X-ray diffraction (PXRD) was performed using Cu K_α radiation with a Philips X'pert diffractometer at room temperature. Chemical compositions and the homogeneousness of the samples were investigated with the energy dispersive X-ray analysis (EDX) of a commercial scanning electron microscope (SEM). The DC magnetic susceptibility was characterized by a superconducting quantum interference device (SQUID) magnetometer. A physical property measurement system (PPMS) was used for AC magnetic susceptibility and electricity transport measurements.

3. Results and Discussion

The parent phase of title DMS is $BaZn_2Sb_2$, a Zintl compound (space group *Pnma*) [35]. Its crystal structure is consisted of ($ZnSb_4$) tetrahedra and insulated Ba cations (Figure 1a). The former is comprised of corner-connected ZnSb chains which are composed by edge sharing ($ZnSb_4$) tetrahedra (Figure 1b–c). In contrast, the crystal structure of *I4mmm*-phase $BaZn_2As_2$ consists of Ba and ZnAs layers, and the latter are formed by edge sharing ($ZnAs_4$) tetrahedral [36].

Rietveld refinement of $(Ba_{0.9}K_{0.1})(Zn_{0.9}Mn_{0.1})_2Sb_2$ is plotted in Figure 1d as a typical example. Refinement parameters and structural details obtained from Rietveld refinement are listed in Table 1. The average bond length of Mn–Sb (2.71 Å) is slightly smaller than that of $BaMn_2Sb_2$ (2.77 Å) [37]. All the peaks of the present samples, $(Ba_{1-x}K_x)(Zn_{0.9}Mn_{0.1})_2Sb_2$ (x = 0, 0.05, 0.075, 0.1, 0.15 and 0.2) and $(Ba_{0.9}K_{0.1})(Zn_{1-y}Mn_y)_2Sb_2$ (y = 0, 0.05, 0.075, 0.1, 0.15 and 0.2) crystallize into the crystal structure of the parent phase. No trace of impurity phase can be found from the lab PXRD patterns. As shown in Figure 1e, the lattice parameters change linearly with doping levels, indicating the successful chemical solutions of Mn [38].

Table 1. Selected structural parameters of $(Ba_{0.9}K_{0.1})(Zn_{0.9}Mn_{0.1})_2Sb_2$ as determined from Rietveld refinements.

Atom	x	y	z	Occupancy	Uiso
Ba	0.2449(2)	0.25	0.3227(1)	0.9	0.0202(6)
K	0.2449(2)	0.25	0.3227(1)	0.1	0.0202(6)
Zn_1	0.0519(3)	0.25	0.6185(3)	0.9	0.0121(10)
Mn_1	0.0519(3)	0.25	0.6185(3)	0.1	0.0121(10)
Zn_2	0.0941(4)	0.25	0.0483(3)	0.9	0.0198(12)
Mn_2	0.0941(4)	0.25	0.0483(3)	0.1	0.0198(12)
Sb_1	0.4774(1)	0.25	0.6636(1)	1.0	0.0162(6)
Sb_2	0.3481(2)	0.25	0.0364(1)	1.0	0.0157(5)

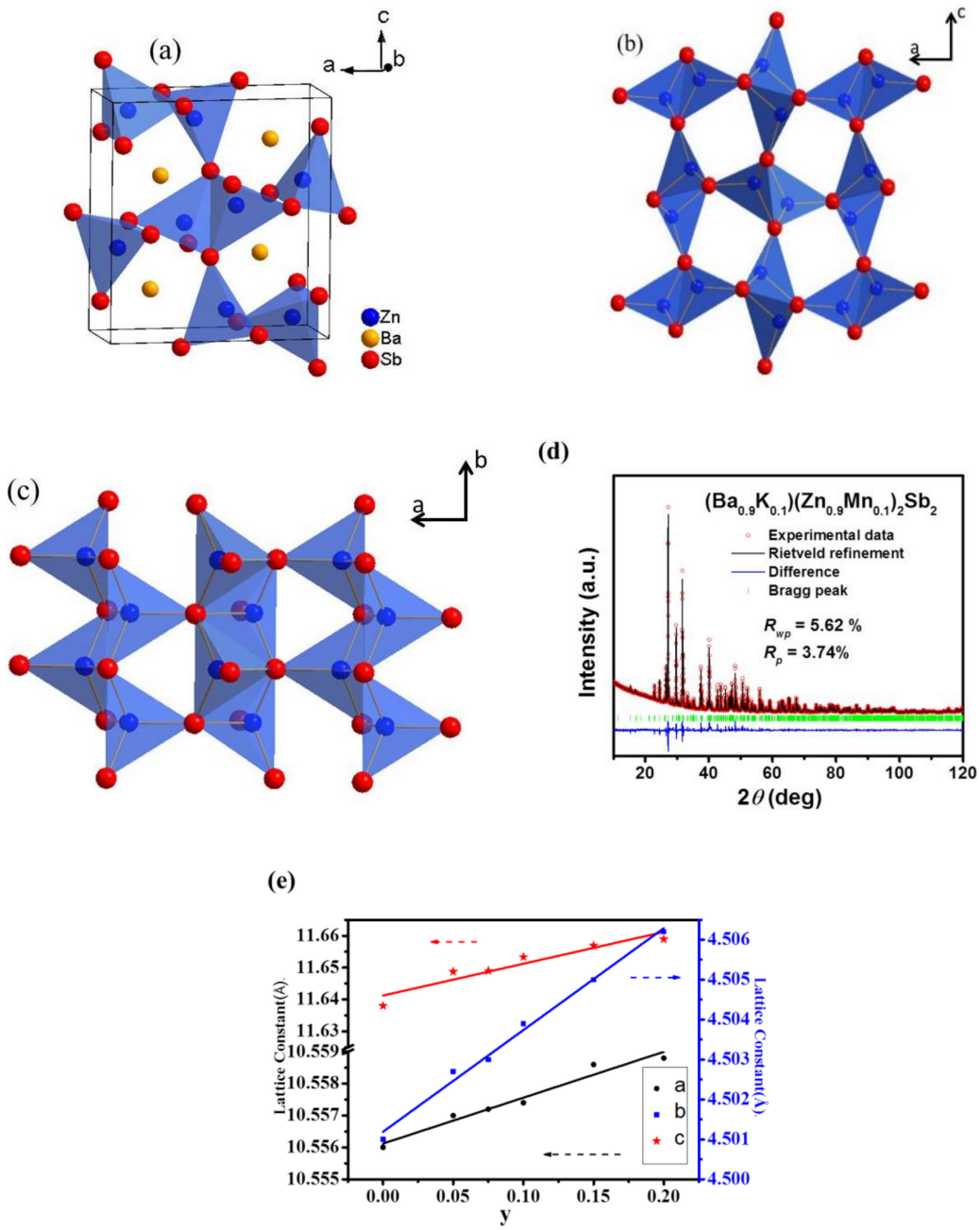

Figure 1. (**a**) Crystal structure of the parent phase, $BaZn_2Sb_2$; (**b**) the sketch of the ZnSb framework in ac-plane; (**c**) the sketch of the ZnSb framework in the ab-plane; (**d**) the Rietveld refinement of $(Ba_{0.9}K_{0.1})(Zn_{0.9}Mn_{0.1})_2Sb_2$; (**e**) the change of the lattice constants, *a* (red dots), *b* (blue dots) and *c* (black dots), with Mn doping levels.

Figure 2a shows the temperature-dependent resistivity ($\rho(T)$) of the parent compound $BaZn_2Sb_2$. The resistivity increases smoothly with increasing temperature from 70 to 220 K, indicating that $BaZn_2Sb_2$ is a weak-degenerate semiconductor [35]. Single Mn-doping increases the resistivity of $Ba(Zn_{1-y}Mn_y)_2Sb_2$ (Figure 2a) due to the possible magnetic scattering effect of Mn^{2+}. In contrast, after doping with a small amount of K into the Ba-site, the resistivity of $(Ba_{0.9}K_{0.1})Zn_2Sb_2$ decreases by about 90% compared to $BaZn_2Sb_2$ (Figure 2b). The role of K-doping is further confirmed by the Hall effect measurements, which will be discussed later. Similar behaviors of $\rho(T)$ are also shown in the K- and Mn-co-doped samples (Figure 2c,d).

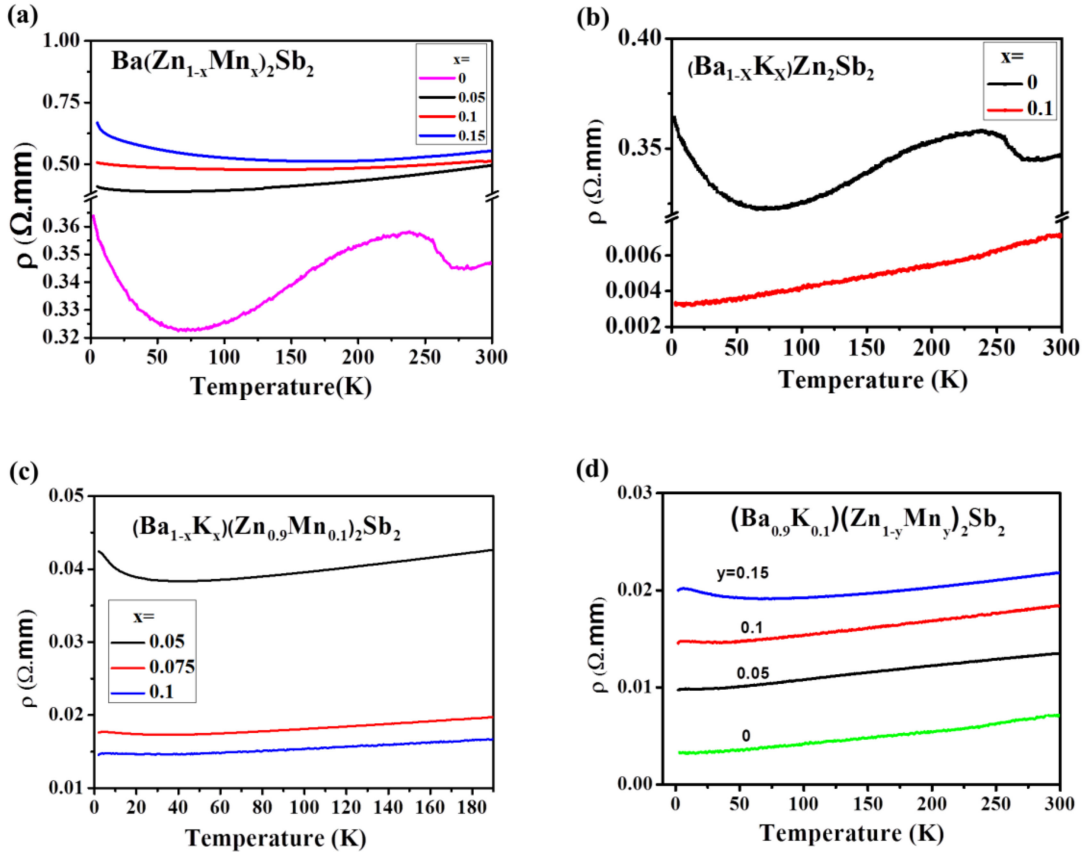

Figure 2. Temperature-dependent resistivity curves of (**a**) $Ba(Zn_{1-y}Mn_y)_2Sb_2$ (y = 0, 0.05, 0.1, 0.15); (**b**) $(Ba_{1-x}K_x)Zn_2Sb_2$; (**c**) $(Ba_{1-x}K_x)(Zn_{0.9}Mn_{0.1})_2Sb_2$ (x = 0.075, 0.1, 0.2); and (**d**) $(Ba_{0.9}K_{0.1})(Zn_{1-y}Mn_y)_2Sb_2$ (y = 0, 0.05, 0.1, 0.15).

With proper doping levels of K and Mn, the title DMSs show spin-glass-like behaviors. Here, we take the sample of $(Ba_{0.925}K_{0.075})(Zn_{0.9}Mn_{0.1})_2Sb_2$ as a typical example to exhibit the spin-glass-like transition. Upon the lowering of the temperature, the DC temperature-dependent magnetization ($M(T)$) of H = 500 Oe shows divergence between zero field cooling and field cooling (T_{irr} ~ 4.7 K) and then one bump (T_S ~ 3.6 K) on zero field cooling in Figure 3a. They rapidly shift towards a lower temperature (T_{irr} ~ 4.1 K and T_S ~ 3.2 K) under H = 1000 Oe. With a higher field of 2000 Oe, the bump on zero field cooling disappears and the divergence between zero field cooling and field cooling could barely be identified. These behaviors indicate spin-glass-like transition [11,39–44]. In Figure 3b, unsaturated "S"-shape field-dependent magnetization ($M(H)$) curves and the presence of hysteresis loop also reveal magnetic frustration. To obtain a closer insight into the glassy magnetism, AC susceptibility under zero field was measured with varying frequencies (f). The results of the sample $(Ba_{0.925}K_{0.075})(Zn_{0.9}Mn_{0.1})_2Sb_2$ are present as typical examples. There is only one transition observed in the real (χ') and imaginary (χ'') parts for each f at about 4.5 K in the temperature range of 2–20 K, consistent with the maximum on the zero field cooling curve. As shown in Figure 3a, the freezing temperature, T_f, moves towards a higher temperature with increasing f on both $\chi'(T)$ and $\chi''(T)$. The f-dependent transition is a typical hallmark of spin-glass-like systems. The frequency shift (K) [43] is calculated to reflect the f-dependence with Equation (1):

$$K = \Delta T_f/[T_f \Delta log(f)]. \quad (1)$$

For a canonical spin-glass system, K ranges between 0.005 and 0.08 [45]. The obtained value of $(Ba_{0.925}K_{0.075})(Zn_{0.9}Mn_{0.1})_2Sb_2$ is K ~ 0.016, indicating the spin-glass nature of $(Ba,K)(Zn,Mn)_2Sb_2$.

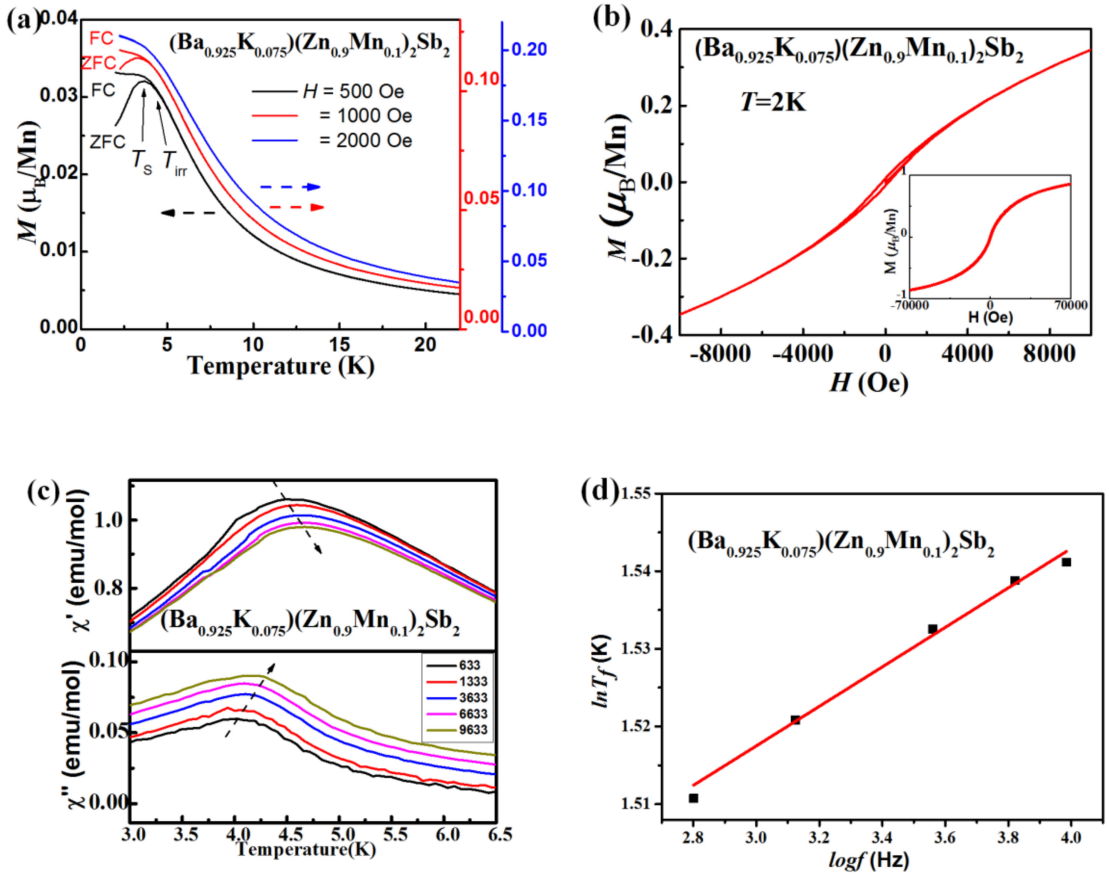

Figure 3. (**a**) DC $M(T)$ measured under H = 500 Oe (black curves), 1000 Oe (red curves) and 2000 Oe (blue curves) of $(Ba_{0.925}K_{0.075})(Zn_{0.9}Mn_{0.1})_2Sb_2$; (**b**) the hysteresis loops at 2 K of $(Ba_{0.925}K_{0.075})(Zn_{0.9}Mn_{0.1})_2Sb_2$; (**c**) AC $\chi'(T)$ and $\chi''(T)$of $(Ba_{0.925}K_{0.075})(Zn_{0.9}Mn_{0.1})_2Sb_2$ at various frequencies; (**d**) frequency dependence of transition temperature of $(Ba_{0.925}K_{0.075})(Zn_{0.9}Mn_{0.1})_2Sb_2$.

To testify the criterion to form spin-glass-like ordering, the DC magnetic behaviors of $(Ba_{0.9}K_{0.1})(Zn_{1-y}Mn_y)_2Sb_2$ (y = 0.05, 0.075, 0.1, 0.15, and 0.2) and $(Ba_{1-x}K_x)(Zn_{0.9}Mn_{0.1})_2Sb_2$ (x = 0.05, 0.075, 0.1, 0.15 and 0.2) are plotted in Figure 4, respectively. In Figure 4a, the sample of y = 0.05 and 0.075 shows no clear magnetic ordering, while the samples with higher Mn concentration behave differently. With increasing temperature, a maximum on the zero field cooling curve and then a divergence between the zero field cooling and field cooling can be found in each sample with y = 0.1, 0.15, and 0.2. In Figure 4b, only the samples with y = 0.1, 0.15, and 0.2 show unsaturated "S"-shape $M(H)$ curves and hysteresis loops. For the sample of y = 0.05 and 0.075, Mn is probably too diluted to build up spin-glass-like ordering. In Figure 4c, spin-glass-like behaviors are present in the sample of $(Ba_{1-x}K_x)(Zn_{0.9}Mn_{0.1})_2Sb_2$ with x = 0.05, 0.075 and 0.1. Surprisingly, further K-doping suppresses the short-range magnetic ordering in the over-doped sample with x ≥ 0.15. The suppression of the short-range magnetic ordering is consistent with $M(H)$ results as shown in Figure 4d. In short, when the concentration of K ≥ 0.2 or the concentration of Mn ≤ 0.075 in $(Ba_{1-x}K_x)(Zn_{1-y}Mn_y)_2Sb_2$, no clear magnetic ordering could be found down to 2 K.

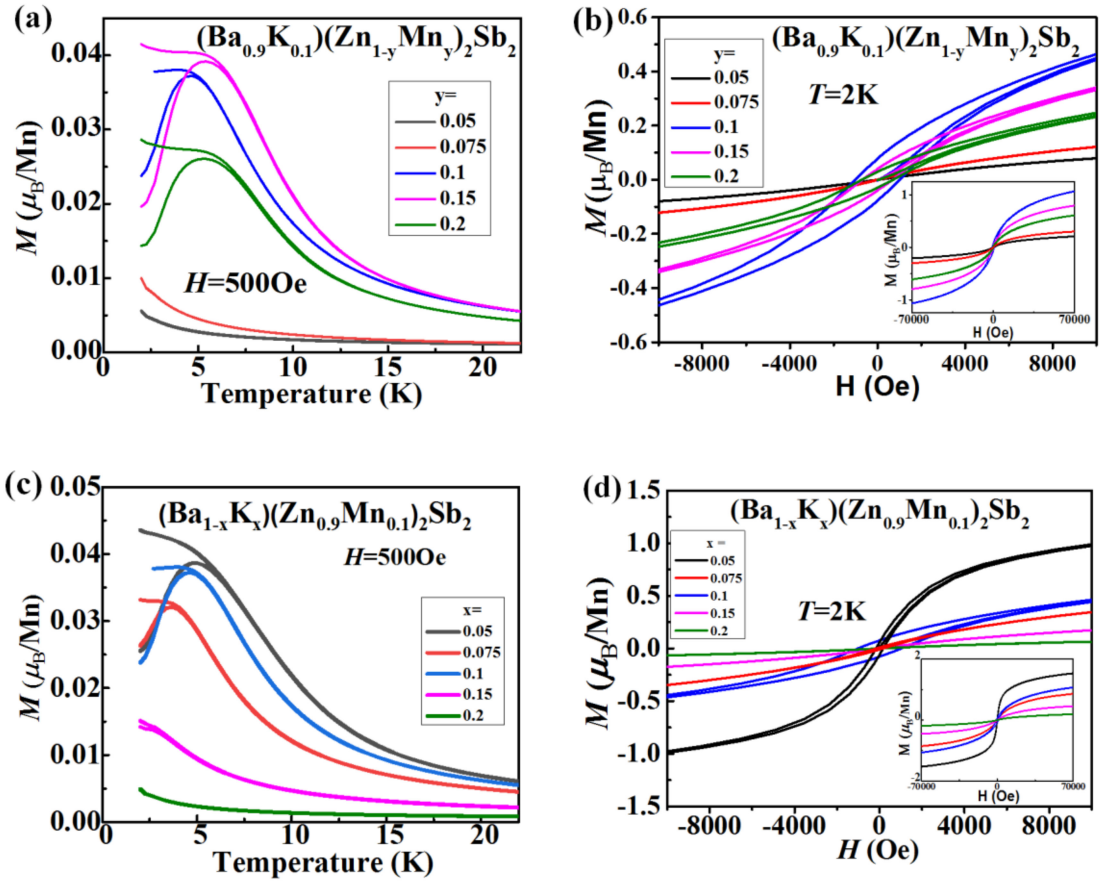

Figure 4. (**a**) DC $M(T)$ measured under H = 500 Oe of $(Ba_{0.9}K_{0.1})(Zn_{1-y}Mn_y)_2Sb_2$ (y = 0.05, 0.075, 0.1, 0.15, 0.2); (**b**) the hysteresis loops at 2 K of $(Ba_{0.9}K_{0.1})(Zn_{1-y}Mn_y)_2Sb_2$; (**c**) $M(T)$ of $(Ba_{1-x}K_x)(Zn_{0.9}Mn_{0.1})_2Sb_2$ (x = 0.05, 0.075, 0.1, 0.15, 0.2) under H = 500 Oe; and (**d**) the hysteresis loops at 2 K of $(Ba_{1-x}K_x)(Zn_{0.9}Mn_{0.1})_2Sb_2$.

Figure 5a shows the $\rho(T)$ curves of $(Ba_{0.9}K_{0.1})(Zn_{0.8}Mn_{0.2})_2Sb_2$ under various fields. Negative magnetoresistance appears around 45 K, which is well above T_f. At H = 0 T, there is a maximum at about 5 K, which is coincident with T_f. On the increasing magnetic field, the maximum shifts toward higher temperature and meanwhile the upturn is gradually suppressed. Figure 5b shows the field-dependent resistivity $\rho(H)$ of $(Ba_{0.9}K_{0.1})(Zn_{0.8}Mn_{0.2})_2Sb_2$ at different temperatures. Magnetoresistance does not saturate up to 7 T at low temperatures (T = 2, 10 and 20 K). The maximum negative magnetoresistance (defined as $\Delta\rho/\rho_0 = ((\rho_H - \rho_0)/\rho_0)$) is 18% at T = 2 K and H = 7 T. Negative magnetoresistance with similar magnitude has been found in many DMS systems, e.g., (Ga,Mn)As, Li(Zn,Mn)As and $(Ba,K)(Zn,Mn)_2As_2$ [5,6,46], where the long-range ferromagnetic ordering is well established. In contrast, negative magnetoresistance in $(Ba_{0.9}K_{0.1})(Zn_{0.8}Mn_{0.2})_2Sb_2$ is related with short-rang spin-glass-like ordering.

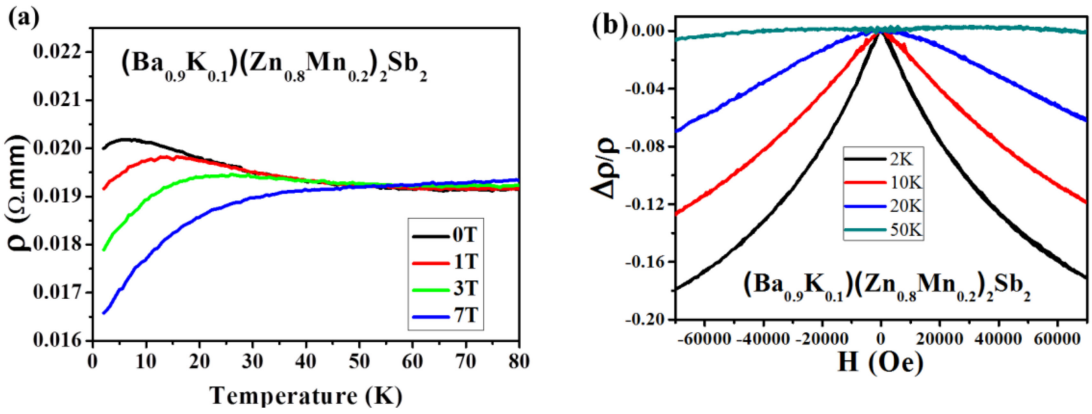

Figure 5. (**a**) $\rho(T)$curves of $(Ba_{0.9}K_{0.1})(Zn_{0.8}Mn_{0.2})_2Sb_2$ under various fields; (**b**) the magnetoresistance curves of $(Ba_{0.9}K_{0.1})(Zn_{0.8}Mn_{0.2})_2Sb_2$ measured in an external field up to 7 T at T = 2 K,10 K, 20 K, 50 K, respectively.

The Hall effect measurements were performed on three typical samples, which are the parent phase $BaZn_2Sb_2$, the K-doped $(Ba_{0.9}K_{0.1})Zn_2Sb_2$ and K- and Mn-co-doped $(Ba_{0.9}K_{0.1})(Zn_{0.9}Mn_{0.1})_2Sb_2$ at T = 2 K and 300 K, respectively. Field-dependent Hall resistivity ($\rho_{xy}(H)$) of $(Ba_{0.9}K_{0.1})(Zn_{0.9}Mn_{0.1})_2Sb_2$ is plotted in Figure 6 as an example. Both low- and high-temperature $\rho_{xy}(H)$ curves are linear in the whole field range (H = 0–7 T). No trace of anomaly Hall effect can be found down to 2 K. Calculated carrier concentrations (n_p) are listed in Table 2. In all the three samples, the major carrier is p-type, and the hole concentrations increase with increasing temperature. The K-doping significantly increases hole concentration (n_p). The obtained carrier concentrations for parent compound $BaZn_2Sb_2$ and $Ba_{0.9}K_{0.1}Zn_2Sb_2$ are about 3×10^{19} cm^{-3} and 4×10^{20} cm^{-3}, respectively. On the other hand, Mn-doping marginally decreases the hole concentration. The n_p of $(Ba_{0.9}K_{0.1})(Zn_{0.9}Mn_{0.1})_2Sb_2$ is less than that of $(Ba_{0.9}K_{0.1})Zn_2Sb_2$ at low temperature. This decrease in n_p is consistent with the increase in resistivity upon Mn doping in Figure 2d.

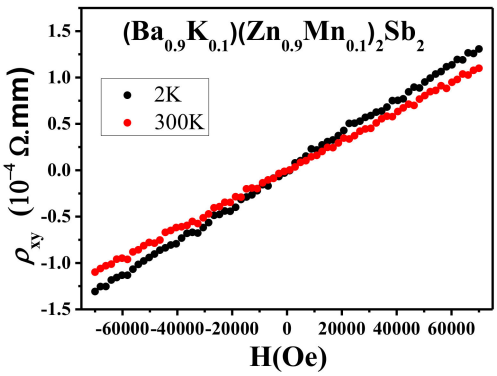

Figure 6. Hall resistivity of $(Ba_{0.9}K_{0.1})(Zn_{0.9}Mn_{0.1})_2Sb_2$ at T = 2 and 300 K.

Although $(Ba,K)(Zn,Mn)_2Sb_2$ and $(Ba,K)(Zn,Mn)_2As_2$ have similar physical properties, including the band gap of parent phases, carrier and spin concentrations, eventually $(Ba,K)(Zn,Mn)_2Sb_2$ forms spin-glass ordering while $(Ba,K)(Zn,Mn)_2As_2$ establish long-range ferromagnetic ordering. The results of $(Ba,K)(Zn,Mn)_2Sb_2$ suggest that more complex factors, for example crystal structure, should be considered to predict magnetism for DMS materials.

Table 2. Calculated carrier concentrations (n_p) of three typical samples.

T (K) \ n_p (cm^{-3})	$BaZn_2Sb_2$	$(Ba_{0.9}K_{0.1})Zn_2Sb_2$	$(Ba_{0.9}K_{0.1})(Zn_{0.9}Mn_{0.1})_2Sb_2$
2	2.73×10^{19}	4.04×10^{20}	3.3×10^{20}
300	3.77×10^{19}	4.11×10^{20}	4.0×10^{20}

4. Conclusions

In summary, a new DMS $(Ba,K)(Zn,Mn)_2Sb_2$ with independent charge and spin doping has been synthesized. With co-doped K and Mn to induce hole carrier and spin, $(Ba,K)(Zn,Mn)_2Sb_2$ can establish a spin-glass ordering at low temperature. A large negative magnetoresistance of 18% related with spin-glass ordering is achieved below freezing temperature. Although $(Ba,K)(Zn,Mn)_2Sb_2$ and ferromagnetic $(Ba,K)(Zn,Mn)_2As_2$ have comparable band gaps, hole and local spin concentrations, they present dramatically different magnetic properties. The title material, $(Ba,K)(Zn,Mn)_2Sb_2$, provides a unique opportunity to testify established DMS models.

Author Contributions: Conceptualization, C.J. and Z.D.; validation, S.Y., Z.D. and C.J.; formal analysis, S.Y., Z.D.; investigation, G.Z., Y.P., X.W., Q.L., R.Y., S.Z. and Y.J.U.; resources, C.J.; data curation, S.Y., J.Z., W.L., and Z.D.; writing—original draft preparation, S.Y.; writing—review and editing, Z.D. and C.J.; supervision, C.J.; project administration, C.J.; funding acquisition, C.J. All authors have read and agreed to the published version of the manuscript.

Funding: This work was financially supported by National Key R&D Program of China (No. 2017YFB0405703), Ministry of Science and Technology of China (2018YFA03057001) and the National Natural Science Foundation of China through the research projects (No. 11921004, 11820101003, 11534016, and 11974407). Z.D. also acknowledges support of the Youth Innovation Promotion Association of CAS (No. 2020007).

Acknowledgments: The authors would like to thank Jianhua Zhao, Xinhui Zhang and Xiaohong Xu for helpful discussions.

Conflicts of Interest: The authors declare no conflict of interest.

References

1. Zutic, I.; Fabian, J.; Das Sarma, S. Spintronics: Fundamentals and applications. *Rev. Mod. Phys.* **2004**, *76*, 323–410. [CrossRef]
2. Jungwirth, T.; Wunderlich, J.; Novák, V.; Olejník, K.; Gallagher, B.L.; Campion, R.P.; Edmonds, K.W.; Rushforth, A.W.; Ferguson, A.J.; Němec, P. Spin-dependent phenomena and device concepts explored in (Ga,Mn)As. *Rev. Mod. Phys.* **2014**, *86*, 855–896. [CrossRef]
3. Erwin, S.C.; Zutic, I. Tailoring ferromagnetic chalcopyrites. *Nat. Mater.* **2004**, *3*, 410–414. [CrossRef] [PubMed]
4. Ohno, H. Making Nonmagnetic Semiconductors Ferromagnetic. *Science* **1998**, *281*, 951–956. [CrossRef]
5. Deng, Z.; Jin, C.Q.; Liu, Q.Q.; Wang, X.C.; Zhu, J.L.; Feng, S.M.; Chen, L.C.; Yu, R.C.; Arguello, C.; Goko, T.; et al. Li(Zn,Mn)As as a new generation ferromagnet based on a I-II-V semiconductor. *Nat. Commun.* **2011**, *2*, 422. [CrossRef] [PubMed]
6. Zhao, K.; Deng, Z.; Wang, X.C.; Han, W.; Zhu, J.L.; Li, X.; Liu, Q.Q.; Yu, R.C.; Goko, T.; Frandsen, B.; et al. New diluted ferromagnetic semiconductor with Curie temperature up to 180 K and isostructural to the '122' iron-based superconductors. *Nat. Commun.* **2013**, *4*, 1442. [CrossRef] [PubMed]
7. Deng, Z.; Zhao, K.; Gu, B.; Han, W.; Zhu, J.L.; Wang, X.C.; Li, X.; Liu, Q.Q.; Yu, R.C.; Goko, T.; et al. Diluted ferromagnetic semiconductor Li(Zn,Mn)P with decoupled charge and spin doping. *Phys. Rev. B* **2013**, *88*, 081203. [CrossRef]
8. Chen, B.J.; Zhao, K.; Deng, Z.; Han, W.; Zhu, J.L.; Wang, X.C.; Liu, Q.Q.; Frandsen, B.; Liu, L.; Cheung, S.; et al. $(Sr,Na)(Zn,Mn)_2As_2$: A diluted ferromagnetic semiconductor with the hexagonal $CaAl_2Si_2$ type structure. *Phys. Rev. B* **2014**, *90*, 155202. [CrossRef]
9. Zhao, K.; Chen, B.J.; Deng, Z.; Han, W.; Zhao, G.Q.; Zhu, J.L.; Liu, Q.Q.; Wang, X.C.; Frandsen, B.; Liu, L.; et al. $(Ca,Na)(Zn,Mn)_2As_2$: A new spin and charge doping decoupled diluted ferromagnetic semiconductor. *J. Appl. Phys.* **2014**, *116*, 163906. [CrossRef]

10. Han, W.; Zhao, K.; Wang, X.C.; Liu, Q.Q.; Ning, F.L.; Deng, Z.; Liu, Y.; Zhu, J.L.; Ding, C.; Man, H.Y.; et al. Diluted ferromagnetic semiconductor (La,Ca)(Zn,Mn)SbO isostructural to "1111" type iron pnictide superconductors. *Sci. China Phys. Mech.* **2013**, *56*, 2026–2030. [CrossRef]
11. Man, H.Y.; Guo, S.L.; Sui, Y.; Guo, Y.; Chen, B.; Wang, H.D.; Ding, C.; Ning, F.L. $Ba(Zn_{1-2x}Mn_xCu_x)_2As_2$: A Bulk Form Diluted Ferromagnetic Semiconductor with Mn and Cu Co-doping at Zn Sites. *Sci. Rep.* **2015**, *5*, 15507. [CrossRef] [PubMed]
12. Ding, C.; Man, H.Y.; Qin, C.; Lu, J.C.; Sun, Y.L.; Wang, Q.; Yu, B.Q.; Feng, C.M.; Goko, T.; Arguello, C.J.; et al. $(La_{1-x}Ba_x)(Zn_{1-x}Mn_x)AsO$: A two-dimensional 1111-type diluted magnetic semiconductor in bulk form. *Phys. Rev. B* **2013**, *88*, 041102. [CrossRef]
13. Chen, B.J.; Deng, Z.; Wang, X.C.; Feng, S.M.; Yuan, Z.; Zhang, S.J.; Liu, Q.Q.; Jin, C.Q. Structural stability at high pressure, electronic, and magnetic properties of BaFZnAs: A new candidate of host material of diluted magnetic semiconductors. *Chin. Phys. B* **2016**, *25*, 077503. [CrossRef]
14. Sun, F.; Li, N.N.; Chen, B.J.; Jia, Y.T.; Zhang, L.J.; Li, W.M.; Zhao, G.Q.; Xing, L.Y.; Fabbris, G.; Wang, Y.G.; et al. Pressure effect on the magnetism of the diluted magnetic semiconductor $(Ba_{1-x}K_x)(Zn_{1-y}M_y)_2As_2$ with independent spin and charge doping. *Phys. Rev. B* **2016**, *93*, 224403. [CrossRef]
15. Sun, F.; Zhao, G.Q.; Escanhoela, C.A.; Chen, B.J.; Kou, R.H.; Wang, Y.G.; Xiao, Y.M.; Chow, P.; Mao, H.K.; Haskel, D.; et al. Hole doping and pressure effects on the II-II-V-based diluted magnetic semiconductor $(Ba_{1-x}K_x)(Zn_{1-y}Mn_y)_2As_2$. *Phys. Rev. B* **2017**, *95*, 094412. [CrossRef]
16. Zhao, G.Q.; Li, Z.; Sun, F.; Yuan, Z.; Chen, B.J.; Yu, S.; Peng, Y.; Deng, Z.; Wang, X.C.; Jin, C.Q. Effects of high pressure on the ferromagnetism and in-plane electrical transport of $(Ba_{0.904}K_{0.096})(Zn_{0.805}Mn_{0.195})_2As_2$ single crystal. *J. Phys.Condens. Mat.* **2018**, *30*, 254001. [CrossRef]
17. Sun, F.; Xu, C.; Yu, S.; Chen, B.J.; Zhao, G.Q.; Deng, Z.; Yang, W.G.; Jin, C.Q. Synchrotron X-Ray Diffraction Studies on the New Generation Ferromagnetic Semiconductor Li(Zn, Mn)As under High Pressure. *Chin. Phys. Lett.* **2017**, *34*, 067501. [CrossRef]
18. Zhao, G.Q.; Lin, C.J.; Deng, Z.; Gu, G.X.; Yu, S.; Wang, X.C.; Gong, Z.Z.; Uemera, Y.J.; Li, Y.Q.; Jin, C.Q. Single Crystal Growth and Spin Polarization Measurements of Diluted Magnetic Semiconductor $(Ba,K)(Zn,Mn)_2As_2$. *Sci. Rep.* **2017**, *7*, 14473. [CrossRef]
19. Wang, R.; Huang, Z.X.; Zhao, G.Q.; Yu, S.; Deng, Z.; Jin, C.Q.; Jia, Q.J.; Chen, Y.; Yang, T.Y.; Jiang, X.M.; et al. Out-of-plane easy-axis in thin films of diluted magnetic semiconductor $Ba_{1-x}K_x(Zn_{1-y}Mn_y)_2As_2$. *AIP Adv.* **2017**, *7*, 045017. [CrossRef]
20. Suzuki, H.; Zhao, G.Q.; Zhao, K.; Chen, B.J.; Horio, M.; Koshiishi, K.; Xu, J.; Kobayashi, M.; Minohara, M.; Sakai, E.; et al. Fermi surfaces and p-d hybridization in the diluted magnetic semiconductor $Ba_{1-x}K_x(Zn_{1-y}Mn_y)_2As_2$ studied by soft x-ray angle-resolved photoemission spectroscopy. *Phys. Rev. B* **2015**, *92*, 235120. [CrossRef]
21. Frandsen, B.A.; Gong, Z.Z.; Terban, M.W.; Banerjee, S.; Chen, B.J.; Jin, C.Q.; Feygenson, M.; Uemura, Y.J.; Billinge, S.J.L. Local atomic and magnetic structure of dilute magnetic semiconductor $(Ba,K)(Zn,Mn)_2As_2$. *Phys. Rev. B* **2016**, *94*, 094102. [CrossRef]
22. Zutic, I.; Zhou, T. Tailoring magnetism in semiconductors. *Sci. China Phys. Mech.* **2018**, *61*, 067031. [CrossRef]
23. Gu, G.X.; Zhao, G.Q.; Lin, C.J.; Li, Y.Q.; Jin, C.Q.; Xiang, G. Asperomagnetic order in diluted magnetic semiconductor $(Ba,Na)(Zn,Mn)_2As_2$. *Appl. Phys. Lett.* **2018**, *112*, 032402. [CrossRef]
24. Anh, L.D.; Kaneko, D.; Hai, P.N.; Tanaka, M. Growth and characterization of insulating ferromagnetic semiconductor (Al,Fe)Sb. *Appl. Phys. Lett.* **2015**, *107*, 232405. [CrossRef]
25. Nam Hai, P.; Duc Anh, L.; Mohan, S.; Tamegai, T.; Kodzuka, M.; Ohkubo, T.; Hono, K.; Tanaka, M. Growth and characterization of n-type electron-induced ferromagnetic semiconductor (In,Fe)As. *Appl. Phys. Lett.* **2012**, *101*, 182403. [CrossRef]
26. Tu, N.T.; Hai, P.N.; Anh, L.D.; Tanaka, M. High-temperature ferromagnetism in heavily Fe-doped ferromagnetic semiconductor (Ga,Fe)Sb. *Appl. Phys. Lett.* **2016**, *108*, 192401. [CrossRef]
27. Tu, N.T.; Hai, P.N.; Anh, L.D.; Tanaka, M. High-temperature ferromagnetism in new n-type Fe-doped ferromagnetic semiconductor (In, Fe) Sb. *Appl. Phys. Express* **2018**, *11*, 063005. [CrossRef]
28. Yamada, Y.; Ueno, K.; Fukumura, T.; Yuan, H.T.; Shimotani, H.; Iwasa, Y.; Gu, L.; Tsukimoto, S.; Ikuhara, Y.; Kawasaki, M. Electrically Induced Ferromagnetism at Room Temperature in Cobalt-Doped Titanium Dioxide. *Science* **2011**, *332*, 1065–1067. [CrossRef]

29. Zhao, K.; Chen, B.; Zhao, G.; Yuan, Z.; Liu, Q.; Deng, Z.; Zhu, J.; Jin, C. Ferromagnetism at 230 K in $(Ba_{0.7}K_{0.3})(Zn_{0.85}Mn_{0.15})_2As_2$ diluted magnetic semiconductor. *Chin. Sci. Bull.* **2014**, *59*, 2524–2527. [CrossRef]
30. Hirohata, A.; Sukegawa, H.; Yanagihara, H.; Zutic, I.; Seki, T.; Mizukami, S.; Swaminathan, R. Roadmap for Emerging Materials for Spintronic Device Applications. *IEEE Trans. Magn.* **2015**, *51*, 0800511. [CrossRef]
31. Glasbrenner, J.K.; Zutic, I.; Mazin, I.I. Theory of Mn-doped II-II-V semiconductors. *Phys. Rev. B* **2014**, *90*, 140403. [CrossRef]
32. Zhao, G.Q.; Deng, Z.; Jin, C.Q. Advances in new generation diluted magnetic semiconductors with independent spin and charge doping. *J. Semicond.* **2019**, *40*, 081505. [CrossRef]
33. Dietl, T.; Ohno, H. Dilute ferromagnetic semiconductors: Physics and spintronic structures. *Rev. Mod. Phys.* **2014**, *86*, 187. [CrossRef]
34. Gu, B.; Maekawa, S. Diluted magnetic semiconductors with narrow band gaps. *Phys. Rev. B* **2016**, *94*, 155202. [CrossRef]
35. Wang, X.-J.; Tang, M.-B.; Zhao, J.-T.; Chen, H.-H.; Yang, X.-X. Thermoelectric properties and electronic structure of Zintl compound $BaZn_2Sb_2$. *Appl. Phys. Lett.* **2007**, *90*, 232107. [CrossRef]
36. Xiao, Z.; Hiramatsu, H.; Ueda, S.; Toda, Y.; Ran, F.Y.; Guo, J.; Lei, H.; Matsuishi, S.; Hosono, H.; Kamiya, T. Narrow bandgap in beta-$BaZn_2As_2$ and its chemical origins. *J. Am. Chem. Soc.* **2014**, *136*, 14959–14965. [CrossRef]
37. Brechtel, E.; Cordier, G.; Schäfer, H. Darstellung und Kristallstruktur von $BaMn_2Sb_2$, $BaZn_2Sb_2$ und $BaCd_2Sb_2$/Preparation and Crystal Structure of $BaMn_2Sb_2$, $BaZn_2Sb_2$ and $BaCd_2Sb_2$. *Zeitschrift für Naturforschung B* **1979**, *34*, 921–925. [CrossRef]
38. Li, W.M.; Cao, L.P.; Zhao, J.F.; Wang, X.C.; Yu, R.Z.; Long, Y.W.; Liu, Q.Q.; Jin, C.Q. Superconductivity of a cuprate with compressed local octahedron. *Sci. China Phys. Mech.* **2019**, *62*, 037421. [CrossRef]
39. Dhar, S.; Brandt, O.; Trampert, A.; Friedland, K.J.; Sun, Y.J.; Ploog, K.H. Observation of spin-glass behavior in homogeneous (Ga,Mn)N layers grown by reactive molecular-beam epitaxy. *Phys. Rev. B* **2003**, *67*, 165205. [CrossRef]
40. Furdyna, J.K. Diluted magnetic semiconductors. *J. Appl. Phys.* **1988**, *64*, R29–R64. [CrossRef]
41. Toliński, T.; Synoradzki, K. Spin-glass behavior in $CeCu_xNi_{4-x}Mn$ and $Ce_{0.9}Nd_{0.1}Ni_4Mn$ compounds. *Intermetallics* **2011**, *19*, 62–67. [CrossRef]
42. Wang, F.; Zhang, J.; Chen, Y.-F.; Wang, G.-J.; Sun, J.-R.; Zhang, S.-Y.; Shen, B.-G. Spin-glass behavior in $La(Fe_{1-x}Mn_x)_{11.4}Si_{1.6}$compounds. *Phys. Rev. B* **2004**, *69*, 094424. [CrossRef]
43. Liu, X.; Matsuishi, S.; Fujitsu, S.; Hosono, H. Spin-glass-like behavior of $CaNi_{1-x}Mn_xGe$. *Phys. Rev. B* **2011**, *84*, 214439. [CrossRef]
44. Macdonald, A.H.; Schiffer, P.; Samarth, N. Ferromagnetic semiconductors: Moving beyond (Ga, Mn)As. *Nat. Mater.* **2005**, *4*, 195–202. [CrossRef]
45. Deng, Z.; Retuerto, M.; Liu, S.Z.; Croft, M.; Stephens, P.W.; Calder, S.; Li, W.M.; Chen, B.J.; Jin, C.Q.; Hu, Z.W.; et al. Dynamic Ferrimagnetic Order in a Highly Distorted Double Perovskite Y_2CoRuO_6. *Chem. Mater.* **2018**, *30*, 7047–7054. [CrossRef]
46. Matsukura, F.; Ohno, H.; Shen, A.; Sugawara, Y. Transport properties and origin of ferromagnetism in (Ga,Mn)As. *Phys. Rev. B* **1998**, *57*, R2037–R2040. [CrossRef]